Tandem fluorescence imaging of dynamic *S*-acylation and protein turnover

Mingzi M. Zhang[1], Lun K. Tsou[1], Guillaume Charron, Anuradha S. Raghavan, and Howard C. Hang[2]

Laboratory of Chemical Biology and Microbial Pathogenesis, The Rockefeller University, New York, NY 10065

Edited* by Carolyn R. Bertozzi, University of California, Berkeley, CA, and approved April 2, 2010 (received for review October 23, 2009)

The functional significance and regulation of reversible *S*-acylation on diverse proteins remain unclear because of limited methods for efficient quantitative analysis of palmitate turnover. Here, we describe a tandem labeling and detection method to simultaneously monitor dynamic *S*-palmitoylation and protein turnover. By combining *S*-acylation and cotranslational fatty acid chemical reporters with orthogonal clickable fluorophores, dual pulse-chase analysis of Lck revealed accelerated palmitate cycling upon T-cell activation. Subsequent pharmacological perturbation of Lck palmitate turnover suggests yet uncharacterized serine hydrolases contribute to dynamic *S*-acylation in cells. In addition to dually fatty-acylated proteins, this tandem fluorescence imaging method can be generalized to other *S*-acylated proteins using azidohomoalanine as a methonine surrogate. The sensitivity and efficiency of this approach should facilitate the functional characterization of cellular factors and drugs that modulate protein *S*-acylation. Furthermore, diverse protein modifications could be analyzed with this tandem imaging method using other chemical reporters to investigate dynamic regulation of protein function.

bioorthogonal ligation | chemical reporters | click chemistry | *S*-palmitoylation | fatty acylation

Protein *S*-palmitoylation (*S*-acylation) targets proteins to discrete intracellular membrane compartments, controls protein stability, and mediates protein-protein interactions (1, 2). Furthermore, the reversibility of *S*-acylation offers spatial and temporal control of protein function akin to protein phosphorylation (Fig. 1*A*). Notably, the differential *S*-palmitoylation and membrane targeting of H- and N-Ras isoforms have been shown to activate discrete signaling pathways for cellular growth and differentiation (3–6). Accelerated deacylation of G-protein subunits and G-protein coupled receptors upon receptor stimulation (7, 8) suggest active mechanisms regulating *S*-acylation/deacylation cycles. In addition, receptor activity-regulated palmitate turnover of PSD-95 is proposed to modulate synaptic strength and plasticity in postsynaptic neurons by mediating receptor clustering (9). Development of the acyl-biotinyl exchange protocol (10–12) and fatty acid chemical reporters (13–16) enabled improved detection and identification of many *S*-palmitoylated proteins from diverse biological pathways in eukaryotes (17). Nonetheless, it remains to be determined if *S*-acylation is dynamic and regulated for identified fatty-acylated proteins.

Quantitative analysis of *S*-acylation/deacylation cycle on proteins would provide further insight into the biological significance and function of dynamic *S*-palmitoylation, but tools to efficiently visualize palmitate turnover on proteins are limited. While photoactivation/bleaching of *S*-palmitoylated proteins fused to fluorescent reporters allow visualization of protein dynamics in cells (4, 5, 18), these methods yield indirect readouts of protein *S*-acylation. Acyl-biotinyl exchange enables nonradioactive detection and enrichment of *S*-acylated proteins (19) but is not ideal for measuring *S*-acylation/deacylation kinetics. Although dual pulse-chase experiments with radioactive (^{3}H, ^{14}C, ^{125}I) fatty acid analogs and [^{35}S]methionine/cysteine are conventionally used to determine deacylation and protein turnover rates, they are cumbersome and require lengthy (weeks to months) detection periods (9). Therefore, more sensitive and efficient methods are needed to accurately monitor dynamic *S*-acylation and protein turnover simultaneously.

Herein, we developed an efficient and fluorescent method for analyzing palmitate turnover as a function of protein turnover in cells. Bioorthogonal ligation reactions, such as the Staudinger ligation or the Cu[1]-catalyzed azide-alkyne cycloaddition (CuAAC) (20), in conjunction with azide- and alkyne-functionalized chemical reporters, afford rapid and sensitive detection of fatty-acylated proteins with higher sensitivity compared with radioactive methods (14, 16). We demonstrated that simultaneous metabolic labeling with two distinct co- and posttranslational chemical reporters followed by sequential on-bead CuAAC reactions using orthogonal fluorescent tags allows robust analysis of palmitate cycling in cells. This approach provides a facile means of comparing the relative palmitate turnover rates on a protein of interest between cellular states or upon pharmacological perturbation. Furthermore, this tandem labeling/detection method is versatile and can be generalized to other *S*-acylated proteins by using different chemical reporters. The ability to simultaneously evaluate both palmitate and protein turnover in a time- and cost-effective manner should facilitate studies of dynamic *S*-acylation in a variety of biological systems.

Results and Discussion

Tandem Fluorescence Imaging Allows Efficient Visualization of *S*-Acylation Turnover on Proteins. To monitor palmitate cycling with fluorescence, we envisioned a pulse-chase experiment that uses distinct chemical reporters with orthogonal readouts (Fig. 1*B*): one to monitor dynamic *S*-acylation and the other to function as an internal control for protein turnover. We initially exploited the chain-length specificity between different fatty acid chemical reporters to orthogonally monitor *S*-palmitoylation and protein synthesis (17). Shorter fatty acid analogs (az-12 and alk-12) preferentially label *N*-myristoylated proteins; the longer fatty acid derivatives (az-15 and alk-16) were incorporated onto *S*-palmitoylated proteins (Fig. 1*C*) (17). Because *N*-myristoylation is primarily a cotranslational and constitutive modification (21), a myristate analog should function as an efficient chemical reporter for the amount and loading of *N*-myristoylated proteins (15, 16). For visualization of two distinct chemical reporters in the same sample, we developed clickable fluorescent detection tags (az/alk-CyFur) based on 2-dicyanomethylene-3-cyano-2,5-dihydrofuran fluorophores (22), which possess near-IR photophysical properties with negligible crosstalk to rhodamine de-

Author contributions: M.M.Z., L.K.T., and H.C.H. designed research; M.M.Z. and L.K.T. performed research; M.M.Z., L.K.T., G.C., and A.S.R. contributed new reagents/analytic tools; M.M.Z., L.K.T., and H.C.H. analyzed data; and M.M.Z., L.K.T., and H.C.H. wrote the paper.

The authors declare no conflict of interest.

*This Direct Submission article had a prearranged editor.

[1]M.M.Z. and L.K.T. contributed equally to this work.

[2]To whom correspondence should be addressed. E-mail: hhang@rockefeller.edu.

This article contains supporting information online at www.pnas.org/lookup/suppl/doi:10.1073/pnas.0912306107/-/DCSupplemental.

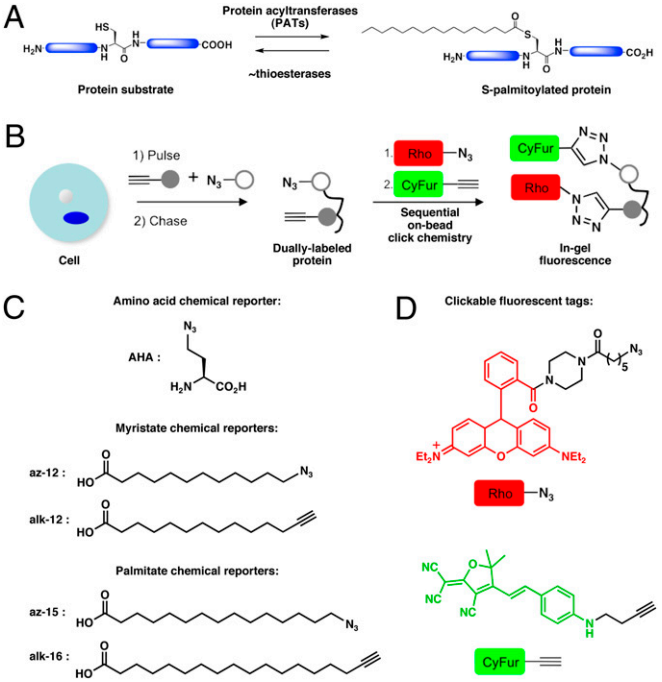

Fig. 1. Tandem fluorescence approach to imaging *S*-palmitoylation turnover on proteins. (*A*) *S*-Palmitoylation is a reversible and dynamic protein modification. (*B*) Following metabolic labeling with two chemical reporters, immunopurification and sequential click chemistry reactions with orthogonal detection tags allow simultaneous visualization of the fatty-acylation and protein synthesis. (*C*) Amino acid chemical reporter for protein synthesis. Fatty acid chemical reporters for *N*-myristoylation and *S*-palmitoylation. (*D*) Clickable fluorescent detection tags.

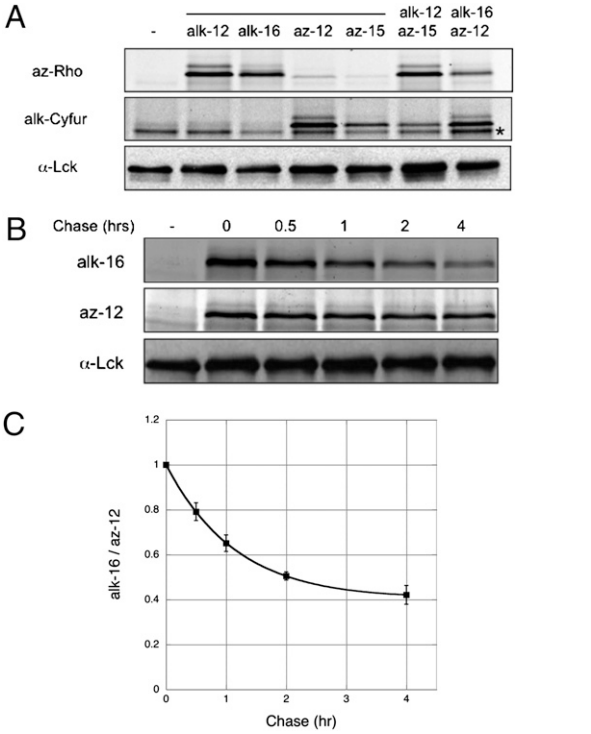

Fig. 2. Analysis of dynamic *S*-palmitoylation on Lck by tandem fluorescence imaging. (*A*) In-gel fluorescence scanning allows tandem detection of az-12 and alk-16 on Lck using alk-Cyfur and az-Rho, respectively. Anti-Lck blot reflects total protein levels. (*B*) Pulse-chase analysis reveals dynamic *S*-palmitoylation of Lck. (*C*) Data from multiple pulse-chase experiments ($n = 10$). Data points from the same chase times, after normalizing alk-16 to az-12 signals, were compiled and displayed as average values ± SEM. *, nonspecific bands.

tection tags (az-Rho/alk-Rho) (Fig. 1*D*). At the same time, we developed protein immunopurification conditions to visualize these orthogonal detection tags by sequential on-bead click chemistry reactions, which allow removal of excess reagents that could interfere with the second CuAAC reaction (Fig. 1*B*).

To explore the simultaneous metabolic labeling and detection of two distinct chemical reporters, we focused on Lck, an *N*-myristoylated and *S*-palmitoylated nonreceptor tyrosine kinase required for T-cell activation (23–25). Lck was immunopurified from Jurkat T cells metabolically labeled with either one or both of the myristate (az-12/alk-12) and palmitate (az-15/alk-16) analogs and subjected to sequential on-bead CuAAC reactions with az-Rho and alk-CyFur. Orthogonal visualization of the two chemical reporters was achieved with in-gel fluorescence scanning. At 532 nm excitation/580 nm emission, az-Rho signal was observed for samples labeled with alkynyl-fatty acid reporters (alk-12 and alk-16); alk-Cyfur fluorescence at 633 nm excitation/670 nm emission was only detected in samples exposed to azido-fatty acid reporters (az-12 and az-15) (Fig. 2*A*). In accordance with biochemical reactivity of thioester and amide linkages (16, 19), in-gel hydroxylamine treatment selectively diminished fluorescence associated with thioester-linked palmitate analogs (az-15/alk-16) compared with amide-linked myristate analogs (az-12/alk-12) (Fig. S1*A*). These results demonstrate that both sets of fatty-acid chemical reporters are specifically incorporated by the respective endogenous *N*-myristoylation and *S*-palmitoylation cellular machinery through native chemical linkages. Our tandem imaging method allows sensitive fluorescent detection of dual-modified proteins from two distinct chemical reporters in parallel. This approach is complementary to copper-mediated and copper-free click-chemistry strategies that have been used for time-resolved imaging of single biosynthetic pathways (26–29).

We then evaluated whether incorporation of alk-16 onto *S*-acylated proteins is reversible in cells and if this tandem labeling/detection method can be used to measure the rate of palmitate cycling on proteins. Lck was immunopurified from Jurkat cells that were pulse-labeled with az-12 and alk-16 followed by a 10-fold excess palmitate chase for different lengths of time. Compared with the relatively constant signal of az-12 labeling of Lck, the fluorescent signal from alk-16 labeling decayed over time (Fig. 2*B* and Fig. S1*B*). No decrease of az-12 signal was observed with excess myristate as the chase additive over 6 h (Fig. S1*C*), demonstrating that az-12 is an effective chemical reporter of constitutive *N*-myristoylation and protein loading. If alk-16 is efficiently recognized by cellular thioesterases, we expect the calculated palmitate half-life on Lck using our method to agree with that of a previously reported pulse-chase study using ^{3}H-palmitate and [^{35}S]methionine (30). After confirming our fluorescence measurements are in the linear range (Fig. S1*D*), our calculated palmitate half-life on Lck is ~50 min (Fig. 2*C*), which is comparable to that reported by Paige et al. under similar experimental conditions (30). Analysis of another fatty-acylated kinase, Fyn (31), from the same lysates, confirmed dual and specific labeling with the fatty acid reporters (Fig. S2 *A* and *B*). The calculated palmitate turnover rate of Fyn is longer than Lck (Fig. S2 *C* and *D*) and is consistent with the reported estimate of 1.5 to 2 h (32). These results demonstrate that the fatty acid reporters and our tandem imaging method can be used to efficiently and accurately evaluate *S*-acylation turnover on endogenously expressed proteins.

Cellular Stimulation by Pervanadate Accelerates Palmitate Cycling on Lck. Because receptor stimulation has been shown to increase palmitate turnover on various proteins, including G-protein sub-

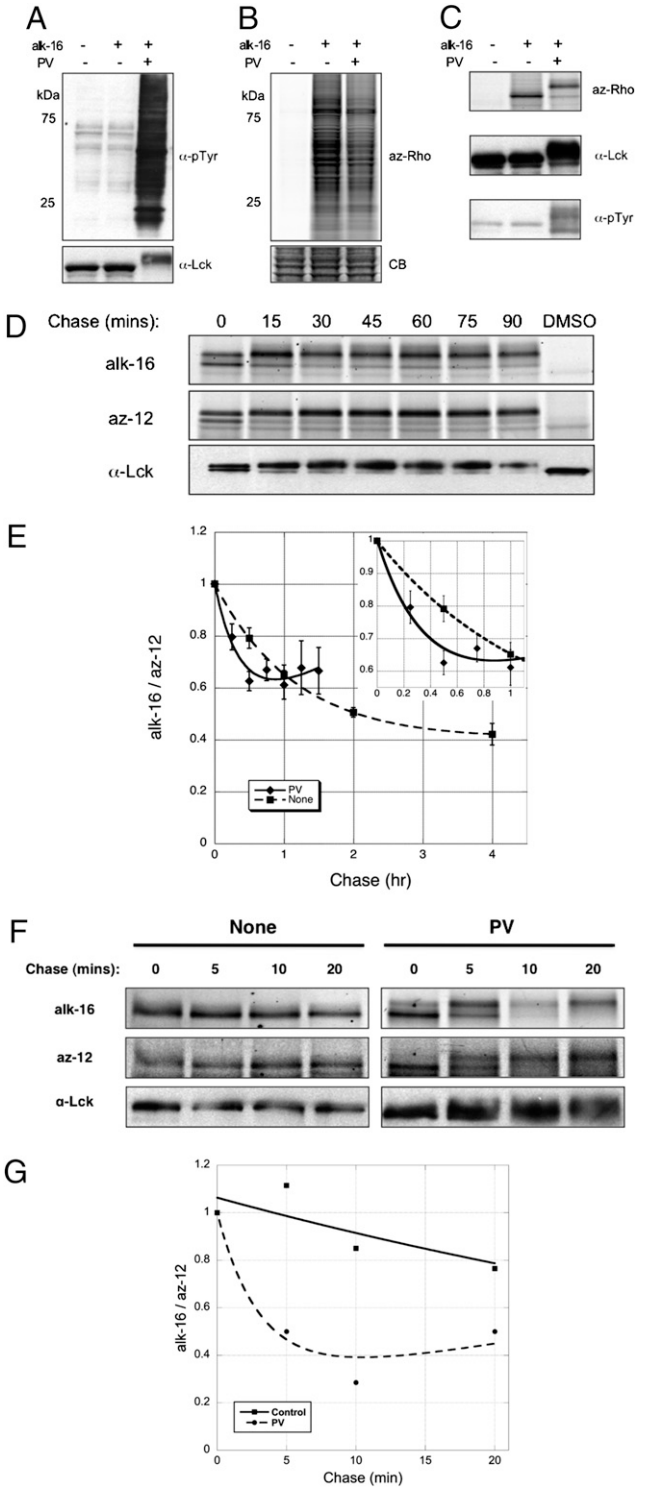

Fig. 3. Pervanadate stimulation of T cells accelerates palmitate cycling on Lck. (*A*) Anti-phosphotyrosine, anti-Lck blots, and (*B*) alk-16 fluorescence of lysates from unstimulated and PV-treated Jurkat T cells. (*C*) Anti-phosphotyrosine, anti-Lck blots, and alk-16 fluorescence of immunopurified Lck from unstimulated and PV-treated Jurkat T cells. Mobility shift of immunopurified Lck was observed with PV treatment. (*D*) Pulse-chase analysis of Lck in the presence of 0.1 mM PV. (*E*) PV activation data from multiple pulse-chase experiments (n = 7). Data points from the same chase times, after normalizing alk-16 to az-12 signals, were compiled and displayed as average values ± SEM (*Inset*). (*F*) Pulse-chase analysis of Lck upon PV treatment with shorter pulse times. (*G*) PV activation data averaged from two pulse-chase experiments with shorter pulse times.

units and G-protein coupled receptors (7–9, 33), and *S*-acylation of Lck is crucial for T-cell activation, we evaluated whether T-cell activation affects palmitate cycling on Lck. We used pervandate (PV), a phosphatase inhibitor, because it has been shown to trigger an activation response similar to that of TCR cross-linking (34). Anti-phosphotyrosine immunoblots revealed substantial increase in protein phosphorylation upon PV treatment (Fig. 3*A*) and mobility shift of phosphorylated Lck was also evident from anti-Lck blots (Fig. 3*B*) and in-gel fluorescence scans (Fig. 3*C*). PV treatment resulted in a 2- to 3-fold increase in palmitate cycling on Lck ($t_{1/2}$ ~15 min) (Fig. 3*D*) that was reproduced over several experiments (n = 7) (Fig. 3*E*), suggesting T-cell activation increases palmitate turnover on Lck.

Palmitate half-life measurements based on pulse-chase experiments that use fatty acid precursors are in the order of minutes or hours, which are often inconsistent with rapid physiological responses that can occur on the seconds time scale. Photo-activation/bleaching of *S*-palmitoylated proteins fused to fluorescent proteins estimate protein-bound palmitate to turnover in milliseconds or seconds (4, 5), but these experiments only measure the trafficking of proteins in cells and do not directly evaluate protein lipidation states. The discrepancy between pulse-chase experiments and imaging studies has been attributed to recycling of labeled fatty acid analogs, even in the presence of large excess of unlabeled substrate during the chase (4, 35). We initially performed 2-hour pulses of the az-12 and alk-16 chemical reporters to compare our results with reported ^{3}H-palmitate pulse-chase studies (30). To address the effects presented by recycling analog pools, we repeated the experiments with shorter pulse-labeling times (30 min) before chasing with excess palmitate (Figs. 3 *F* and *G*), which has been demonstrated to minimize recycling of substrates in pulse-chase studies (35). The absolute fluorescence intensities observed for both az-12 and alk-16 were lower overall, but they remained in the linear range (Fig. S1*D*). Consistent with less recycling of alk-16, shorter pulses yielded a faster palmitate half-life of ~30 min on Lck compared with the ~50 min obtained with longer 2-hour pulses (Figs. S3 *A* and *B*) and the normalized alk-16 signal plateaus at a lower level with shorter pulses (Fig. S3*B*). The increase in palmitate turnover on Lck upon PV stimulation, however, persists with shorter pulse times (Fig. 3*F*), with an estimated half-life of <5 min (Fig. 3*G*). Notably for PV-treated cells, recovery of alk-16 signal was observed even with a shorter pulse time (Fig. 3*F*), which can be attributed to the rapid recycling of alk-16. These results demonstrate our tandem imaging method can reveal rapid rates of palmitate cycling on proteins that are closer to values obtained using fluorescence microscopy (36) and confirms that T-cell stimulation with PV accelerates palmitoylation cycling on Lck.

Faster depalmitoylation of Lck upon T-cell activation raises several interesting questions with regard to dynamic *S*-acylation. Although *S*-palmitoylation of enzymes (Lck) and adaptor proteins (LAT) is critical for proper T-cell activation (37, 38), the dynamic nature of *S*-acylation during cellular stimulation on these proteins is unclear. Site-directed mutagenesis studies on key cysteine residues demonstrate that non-acylated Lck is not targeted to the plasma membrane (39). Further evidence suggests that *S*-acylation of Lck is not solely a membrane targeting mechanism. An Lck chimera fused to the transmembrane domain of CD4, which targets it to the plasma membrane, shows reduced association with lipid rafts and decreased T-cell signaling activity (37). Introduction of a more hydrophilic oxygen-substituted palmitate analog on Lck also results in weaker TCR signaling (40). Live cell-imaging studies of Lck-GFP during T-cell activation suggest that Lck is dynamically recruited and distributed to the periphery of immunological synapses (41). It is therefore possible that increased palmitate turnover upon T-cell activation may serve to limit the proportion of raft-associated Lck and mediate the accessibility of Lck to its substrates or

activators. A possible explanation is that protein thioesterase activity is stimulated by downstream effects of TCR signaling, such as release of calcium from intracellular stores in the endoplasmic reticulum. Alternatively, activated Lck may assume a conformational change favorable toward spontaneous or enzymatic deacylation. Because protein thioesterases with deacylating activity toward Lck are yet to be identified, mechanistic insights into the regulation of activity-induced palmitate turnover remain elusive.

Pharmacological Perturbation of Palmitate Cycling on Lck. Efforts to identify enzymes that can deacylate proteins have suggested a cytosolic acyl protein thioesterase-1 (APT1) and a lysosomal palmitoyl-protein thioesterase-1 (PPT1) as candidate depalmitoylating enzymes (42, 43). Because both enzymes are predicted to be serine hydrolases based on sequence homology and structure studies, we investigated the effect of a broad-spectrum serine hydrolase inhibitor on Lck depalmitoylation. Addition of methyl arachidonyl fluorophosphonate (MAFP) during the chase significantly retarded palmitate turnover on Lck (Fig. 4), suggesting that serine hydrolases sensitive toward the reactive fluorophosphonate group of MAFP may contribute to the deacylation of Lck in T cells. In contrast, incubation with another broad-spectrum serine hydrolase inhibitor, phenylmethylsulfonyl fluoride (PMSF) had no apparent effect on the initial rate of palmitate removal (Fig. S4). Structural studies suggest that the bulky aromatic group of PMSF sterically hinders its binding to the active site of lipid serine hydrolases, such as PPT1 (44). Because PPT1 resides in lysosomal compartments that are not topologically compatible with cytosolic deacylation reactions, and APT1 deacylation activity has only been demonstrated in vitro with limited substrates, enzymes that deacylate proteins in cells remain unclear. Nonetheless, our results with mechanism-based inhibitors suggest that serine hydrolases with active sites similar to that of PPT1 may contribute to the observed thioesterase activity on Lck.

We also assessed the effect of 2-bromopalmitate (2BP), a palmitoyltransferase inhibitor commonly used to block *S*-acylation (45, 46). Interestingly, 2BP also decreased Lck depalmitoylation rate (Fig. 4). The actual targets of 2BP in cells are unknown and enzymes other than palmitoyltransferases have been suggested to interact with 2BP (47). It is possible that 2BP, which harbors a reactive α-bromo-carboxyl functional group poised for nucleophilic attack, might also inhibit putative thioesterases. This theory raises concerns over the use of 2BP as a specific palmitoyltransferase inhibitor in cells and subsequent interpretation of data using 2BP. Collectively, these experiments demonstrate that such a dual detection method can be used to evaluate effects of chemical inhibitors on palmitate turnover. Development of more specific inhibitors using this assay should facilitate discovery and characterization of cellular factors that perturb palmitate turnover in cells.

Generality of the Tandem Imaging Method for *S*-Acylated Proteins. To evaluate the utility of our tandem imaging method beyond *N*-myristoylated proteins, we used a general chemical reporter of protein synthesis. Azidohomoalanine (AHA), a well-described azide-bearing methionine surrogate shown to label newly synthesized proteins with no observed toxicity, is an attractive alternative (48, 49). We used an HA-tagged H-Ras^{G12V} construct to analyze another class of *S*-acylated proteins. In-gel fluorescence analysis of purified HA-tagged H-Ras^{G12V} expressed in HeLa cells that were metabolically labeled with alk-16 and AHA showed incorporation and orthogonal detection of both chemical reporters (Fig. S5*A*). We then compared our tandem imaging pulse-chase data with reported radioactive studies of H-Ras variants (50). Palmitate removal rates on oncogenic H-Ras isoforms have been experimentally shown to be ~1 h (50). Pulse-chase analysis revealed significantly faster chase kinetics for alk-16 than AHA, demonstrating dynamic *S*-acylation and minimal turnover of H-Ras^{G12V} in the time points analyzed (Fig. 5*A* and Fig. S5*B*). The HA-tagged H-Ras^{G12V} construct appeared as doublets by Cyfur fluorescence and anti-HA Western blot, but only the upper band is modified by alk-16 as observed with az-Rho fluorescence (Fig. 5*A*), suggesting the slower migrating polypeptide is the lipid-modified isoform of H-Ras^{G12V} under these conditions. Average

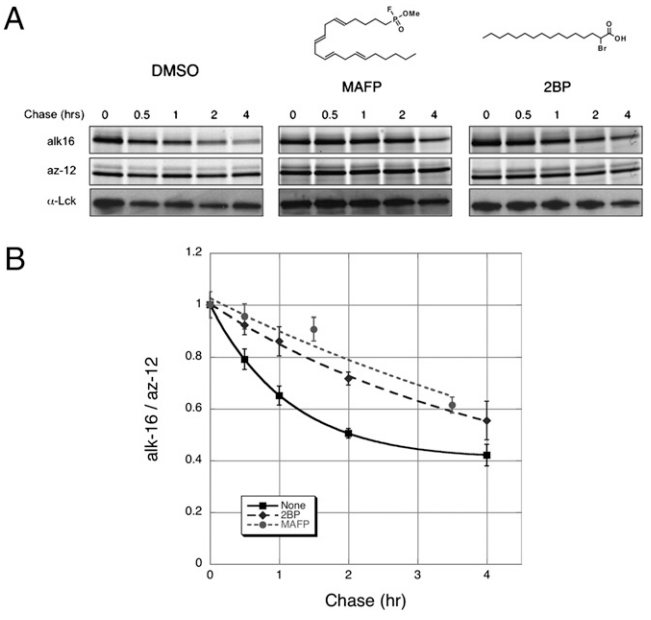

Fig. 4. Pharmacological perturbation of palmitate turnover on Lck. (*A*) Pulse-chase analysis of Lck in the presence of chemical inhibitors. (*B*) Data from multiple pulse-chase experiments (n = 2). Data points from the same chase times, after normalizing alk-16 to az-12 signals, were compiled and displayed as average values ± SEM.

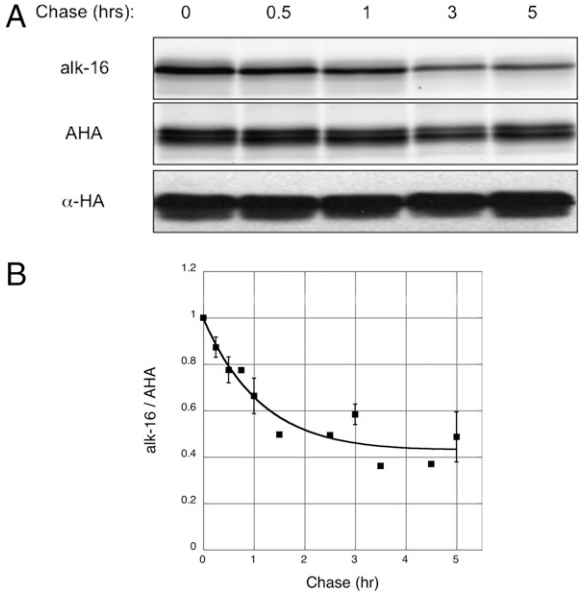

Fig. 5. Use of a more general protein synthesis chemical reporter extends the tandem imaging method beyond *N*-myristoylated proteins. (*A*) Pulse-chase analysis of H-Ras^{G12V} upon labeling with AHA and alk-16. (*B*) Data from multiple pulse-chase experiments (n = 5). Data points from the same chase times, after normalizing alk-16 to AHA signals, were compiled and displayed as average values ± SEM.

Cyfur fluorescence across both H-Ras^{G12V} isoforms was used for data normalization, as both exhibited similar turnover rates. The palmitate half-life on H-Ras^{G12V} was calculated to be ~50 min with our tandem imaging method over several experiments ($n = 5$) (Fig. 5*B*). This finding is consistent with the reported experimental palmitate turnover rates of other oncogenic H-Ras variants (50). Based upon these experimental rates of palmitate cycling and GTP-binding measurements, the calculated palmitate half-life of fully GTP-bound H-Ras is less than 10 min (50). The combined use of alk-16 with AHA should enable tandem fluorescence imaging of palmitate turnover on any *S*-acylated protein.

Conclusions

Sensitive and efficient methods are needed to measure dynamic changes of posttranslational modifications to fully appreciate their roles in cell signaling. *S*-Palmitoylation is a reversible form of protein lipidation that has been difficult to study because of limitations in monitoring *S*-acylation/deacylation. We therefore developed a tandem labeling and fluorescence imaging method using two orthogonal chemical reporters to simultaneous monitor palmitate cycling rates and protein turnover. Our method provides rapid and sensitive fluorescent detection of palmitate cycling rates within linear dynamic ranges and internally normalized measurement of protein levels. This approach should be applicable to any *S*-acylated proteins of interest to readily monitor changes in palmitate cycling upon cellular stimulation or in response to pharmacological perturbations. We envision the strategy to be useful in uncovering cellular factors regulating the *S*-acylation/deacylation cycle, including putative thioesterases with in vivo deacylating activity. Finally, given its modularity and the wide spectrum of chemical reporters currently available (20), this tandem imaging approach can be readily adapted to study other dynamic protein modifications.

Materials and Methods

Cell Culture Growth. Jurkat (human T-cell lymphoma) cells were propagated in RMPI 1640 supplemented with 10% FBS, 100 U/mL penicillin and 100 μg/mL streptomycin in a humidified CO_2 incubator at 37 °C. Cell densities were maintained between 1×10^5 and 2×10^6 cells per milliliter. HeLa cells were cultured in DMEM, supplemented with 10% FBS (FBS), 100 U/mL penicillin with 100 μg/mL streptomycin and maintained in a humidified 37 °C incubator with 5% CO_2.

Transfection of N-Terminal HA-Tagged H-Ras^{G12V}. For transfection studies, HeLa cells were grown in a 10-cm culture plate supplemented with DMEM containing 10% FBS in a humidified CO_2 incubator to ≈90% confluence before transfection with 12 to 15 μg of DNA using Lipofectamine 2000 (Invitrogen). The N-terminal HA-tagged H-Ras^{G12V} (PCNC10) construct was kindly provided by Marilyn Resh (Memorial Sloan-Kettering Cancer Center). Cells were transfected about 16 h before metabolic labeling and subsequent chase conditions, as described below.

Pulse-Chase Metabolic Labeling. Jurkat T cells were labeled with 20 μM az-12 and 20 μM alk-16 in RMPI 1640 supplemented with 2% charcoal-filtered FBS, 100 U/mL penicillin, and 100 μg/mL streptomycin. Similarly for H-Ras studies, transfected HeLa cells were incubated with 1 mM AHA and 20 μM alk-16 in methonine-free DMEM (Invitrogen) supplemented with 2% charcoal-filtered FBS. The same volume of DMSO was used in the negative controls. After 2 h or 30 min incubation, the labeled cells were chased with prewarmed RMPI 1640 or DMEM containing 200 μM palmitate, 10% FBS or 100 U/mL penicillin, and 100 μg/mL 100 μM 2BP (Fluka), 20 μM (MAFP) (Sigma), or 200 μM PMSF were added to the chase medium to investigate the effects of small-molecule inhibitors on palmitate turnover. To determine palmitate turnover upon T-cell activation, 100 mM pervanadate, prepared by dissolving sodium orthovanadate in 300 mM H_2O_2, was added to the chase medium for a final pervanadate concentration of 0.1 mM. Samples were taken at various time points during the chase, washed once with cold PBS, and flash-frozen in liquid nitrogen before storage at −80 °C.

Preparation of Cell Lysates. Frozen Jurkat or HeLa cell pellets were lysed in chilled Brij lysis buffer (1% Brij-97, 150 mM NaCl, 50 mM triethanolamine pH 7.4, 10× Roche EDTA-free protease inhibitor mixture, 10 mM PMSF) with vigorous vortexing (3 × 20 s), placing tubes on ice during intervals to avoid heating of samples. For T-cell activation studies, 1:50 dilution of phosphatase inhibitor mixture 2 (Sigma) was included in the lysis buffer. Lysates were spun at 1,000 × *g* for 5 min at room temperature to remove cellular debris. Typical lysate concentrations of 4 to 8 mg/mL were obtained, as quantified using the BCA assay (Pierce).

Immunoprecipitations. Lck and Fyn proteins were immunoprecipitated from 0.8 to 1 mg of Jurkat cell lysate using a mouse anti-Lck (p56^{Lck}) monoclonal (Clone 3A5, Invitrogen) and a rabbit anti-Fyn polyclonal (Upstate), respectively. Twenty-five microliters of packed Agarose A beads (Roche) was used for each sample. For HA-tagged H-Ras^{G12V} analysis, 15 μL of anti-HA beads (monoclonal anti-HA agarose conjugate, clone HA-7) was added to 200 to 300 μg of HeLa cell lysates. After 2 h incubation on a platform rocker at 4 °C, the beads were washed three times with 1 mL of ice-cold RIPA buffer (1% Triton X-100, 1% sodium deoxycholate, 0.1% SDS, 50 mM triethanolamine pH 7.4, 150 mM NaCl) before sequential on-bead click chemistry.

Sequential On-Bead CuAAC/Click Chemistry. The beads were resuspended in 20 μL of PBS and 2.25 μL freshly premixed click-chemistry reaction mixture [az-Rho (100 μM, 5 mM stock solution in DMSO), Tris(2-carboxyethyl)phosphine hydrochloride (TCEP) (1 mM, 50 mM freshly prepared stock solution in deionized water), Tris[(1-benzyl-1*H*-1,2,3-triazol-4-yl)methyl]amine (TBTA) (100 μM, 2 mM stock solution in 1:4 DMSO:t-butanol) and $CuSO_4 \cdot 5H_2O$ (1 mM, 50 mM freshly prepared stock solution in deionized water)] for a total approximate reaction volume of 25 μL for 1 h at room temperature. The beads were washed three times with 1 mL of ice-cold RIPA buffer (1% Triton X-100, 1% sodium deoxycholate, 0.1% SDS, 50 mM triethanolamine pH 7.4, 150 mM NaCl) and resuspended in 20 μL of SDS buffer (4% SDS, 50 mM triethanolamine pH 7.4, 150 mM NaCl). Next, 2.25 μL of freshly premixed click-chemistry reagents (alk-Cyfur in place of az-Rho) were added. After 1 h at room temperature, the reaction mixture was diluted with 8.7 μL 4× reducing SDS-loading buffer (40% glycerol, 200 mM Tris·HCl pH 6.8, 8% SDS, 0.4% bromophenol blue) and 1.3 μL 2-mercaptoethanol, heated for 5 min at 95 °C, and 20 μL was loaded per gel lane for separation by SDS/PAGE (4–20% Bio-Rad Criterion Tris-HCl gel). A separate gel was loaded for Western blot analysis.

In-Gel Fluorescence Scanning. Proteins separated by SDS/PAGE were visualized by incubating the gel in 40% methanol, 10% acetic acid for at least 1 h and directly scanning it on a GE Healthcare Typhoon 9400 variable-mode imager. Rhodamine-associated signal was detected at excitation 532 nm/emission 580 nm; orthogonal detection of Cyfur-associated signal was achieved at excitation 633 nm/emission 670 nm.

Hydroxylamine Treatment of Gels. After an initial fluorescence scan to determine pretreatment fluorescence, the gel was rinsed with deionized water and soaked in freshly prepared 1 M NH_2OH (pH 7.4) for 2 h at room temperature on a shaker. The gel was subsequently rinsed with deionized water and incubated with shaking for 2 h in 40% methanol and 10% acetic acid at room temperature before scanning for posttreatment fluorescence.

Western Blots. Proteins separated by SDS/PAGE were transferred to nitrocellulose membranes (50 mM Tris, 40 mM glycine, 0.0375% SDS, 20% MeOH in deionized water, Bio-Rad Trans-Blot Semi-Dry Cell, 20 V, 40 min), which were blocked with 10% nonfat milk, 2% BSA, 0.1% Tween-20 in PBS (0.1% PBST) and washed with 0.1% PBST before incubation with appropriate antibodies. Membranes were incubated with a mouse anti-Lck (p56^{Lck}) monoclonal (Clone 3A5, Invitrogen) followed by light chain-specific HRP-conjugated affiniPure goat anti-mouse secondary (Jackson Immunoresearch Laboratories) for anti-Lck blots. Likewise, anti-Fyn blots were treated with mouse anti-Fyn monoclonal (Clone 1S, Chemicon) followed by goat anti-mouse HRP-conjugated secondary antibody (Upstate). Anti-HA blots were treated with rabbit anti-HA polyclonal (Clontech) followed by goat anti-rabbit HRP-conjugated secondary antibody (Upstate). Anti-phosphotyrosine blots were blocked with 5% BSA in 0.1% PBST before incubation with HRP-conjugated anti-phosphotyrosine mouse monoclonal (PY99, Santa Cruz). Blots were developed using the enhanced chemiluminescent kit (GE Healthcare).

Image Processing and Calculations. All images were processed and analyzed using the ImageJ software. A rectangular box was tightly selected around the bands of interest and average fluorescence intensity at midlength of the box was measured. Dimensions of the box were maintained within the same experiment. No event of signal saturation was observed in this study. Background signal from nonspecific labeling was removed by subtracting measurements of the DMSO sample from each of the datapoints. The ratio of background-

corrected alk-16 to az-12 associated fluorescent signals accounted for protein load and turnover at each time point of a pulse-chase analysis. To allow comparison between pulse-chase experiments, alk-16/az-12 values within each dataset were normalized such that alk-16/az-12 = 1 at T = 0 h, which was defined as the earliest of three consecutive time points during which a decrease of alk-16/az-12 was initially observed. Because values obtained under some conditions tested did not form a straight line when plotted on a logarithmic scale, which was observed by others (50), data for each protein or chase condition was fitted to a two-phase exponential decay model using the KaleidaGraph graphing and data analysis software. The equation used was a biphasic exponential decay line $m1 \times \exp(-m2 \times m0) + m3 \times \exp(-m4 \times m0)$, which starts at m1 + m3 and decays with rate constants m2 and m4. The half-life of protein-bound palmitate ($t_{1/2}$) was defined as the length time required for the normalized alk-16/az-12 signal to decrease halve if decay was to occur solely at the initial rate, which is ln(2)/m2, with m1 = 0.5.

ACKNOWLEDGMENTS. We thank members of the H.C.H. laboratory and Dr. Marilyn Resh for reagents and constructs. M.M.Z. is supported by the Agency for Science, Technology and Research, Singapore. L.K.T. acknowledges support from The Rockefeller University Marie-Josée and Henry Kravis Postdoctoral Fellowship. G.C. thanks the Rockefeller/Sloan-Kettering/Cornell Tri-Institutional Program in Chemical Biology. A.R. thanks the New York Community Trust-Heiser Grant for a postdoctoral fellowship. H.C.H. acknowledges support from The Rockefeller University, Irma T. Hirschl/Monique Weill-Caulier Trust, and the Ellison Medical Foundation.

1. Resh MD (2006) Trafficking and signaling by fatty-acylated and prenylated proteins. *Nat Chem Biol* 2:584–590.
2. Linder ME, Deschenes RJ (2007) Palmitoylation: Policing protein stability and traffic. *Nat Rev Mol Cell Biol* 8:74–84.
3. Onken B, Wiener H, Philips MR, Chang EC (2006) Compartmentalized signaling of Ras in fission yeast. *Proc Natl Acad Sci USA* 103:9045–9050.
4. Rocks O, et al. (2005) An acylation cycle regulates localization and activity of palmitoylated Ras isoforms. *Science* 307:1746–1752.
5. Goodwin JS, et al. (2005) Depalmitoylated Ras traffics to and from the Golgi complex via a nonvesicular pathway. *J Cell Biol* 170:261–272.
6. Quatela SE, Philips MR (2006) Ras signaling on the Golgi. *Curr Opin Cell Biol* 18: 162–167.
7. Loisel TP, Adam L, Hebert TE, Bouvier M (1996) Agonist stimulation increases the turnover rate of beta 2AR-bound palmitate and promotes receptor depalmitoylation. *Biochemistry* 35:15923–15932.
8. Degtyarev MY, Spiegel AM, Jones TL (1993) Increased palmitoylation of the Gs protein alpha subunit after activation by the beta-adrenergic receptor or cholera toxin. *J Biol Chem* 268:23769–23772.
9. El-Husseini Ael-D, et al. (2002) Synaptic strength regulated by palmitate cycling on PSD-95. *Cell* 108:849–863.
10. Kang R, et al. (2008) Neural palmitoyl-proteomics reveals dynamic synaptic palmitoylation. *Nature* 456:904–909.
11. Roth AF, et al. (2006) Global analysis of protein palmitoylation in yeast. *Cell* 125: 1003–1013.
12. Yang W, Di Vizio D, Kirchner M, Steen H, Freeman MR (2010) Proteome-scale characterization of human s-acylated proteins in lipid raft-enriched and non-raft membranes. *Mol Cell Proteomics* 9:54–70.
13. Hannoush RN, Arenas-Ramirez N (2009) Imaging the lipidome: Omega-alkynyl fatty acids for detection and cellular visualization of lipid-modified proteins. *ACS Chem Biol* 4:581–587.
14. Martin BR, Cravatt BF (2009) Large-scale profiling of protein palmitoylation in mammalian cells. *Nat Methods* 6:135–138.
15. Hang HC, et al. (2007) Chemical probes for the rapid detection of fatty-acylated proteins in mammalian cells. *J Am Chem Soc* 129:2744–2745.
16. Charron G, et al. (2009) Robust fluorescent detection of protein fatty-acylation with chemical reporters. *J Am Chem Soc* 131:4967–4975.
17. Charron G, Wilson J, Hang HC (2009) Chemical tools for understanding protein lipidation in eukaryotes. *Curr Opin Chem Biol* 13:382–391.
18. Kanaani J, Patterson G, Schaufele F, Lippincott-Schwartz J, Baekkeskov S (2008) A palmitoylation cycle dynamically regulates partitioning of the GABA-synthesizing enzyme GAD65 between ER-Golgi and post-Golgi membranes. *J Cell Sci* 121:437–449.
19. Drisdel RC, Green WN (2004) Labeling and quantifying sites of protein palmitoylation. *Biotechniques* 36:276–285.
20. Sletten EM, Bertozzi CR (2009) Bioorthogonal chemistry: Fishing for selectivity in a sea of functionality. *Angew Chem Int Ed Engl* 48:6974–6998.
21. Johnson DR, Bhatnagar RS, Knoll LJ, Gordon JI (1994) Genetic and biochemical studies of protein N-myristoylation. *Annu Rev Biochem* 63:869–914.
22. Tsou LK, Zhang MM, Hang HC (2009) Clickable fluorescent dyes for multimodal bioorthogonal imaging. *Org Biomol Chem* 7:5055–5058.
23. Rodgers W, Crise B, Rose JK (1994) Signals determining protein tyrosine kinase and glycosyl-phosphatidylinositol-anchored protein targeting to a glycolipid-enriched membrane fraction. *Mol Cell Biol* 14:5384–5391.
24. Koegl M, Zlatkine P, Ley SC, Courtneidge SA, Magee AI (1994) Palmitoylation of multiple Src-family kinases at a homologous *N*-terminal motif. *Biochem J* 303: 749–753.
25. Shenoy-Scaria AM, Gauen LK, Kwong J, Shaw AS, Lublin DM (1993) Palmitylation of an amino-terminal cysteine motif of protein tyrosine kinases p56lck and p59fyn mediates interaction with glycosyl-phosphatidylinositol-anchored proteins. *Mol Cell Biol* 13:6385–6392.
26. Beatty KE, Tirrell DA (2008) Two-color labeling of temporally defined protein populations in mammalian cells. *Bioorg Med Chem Lett* 18:5995–5999.
27. Kele P, Mezö G, Achatz D, Wolfbeis OS (2009) Dual labeling of biomolecules by using click chemistry: A sequential approach. *Angew Chem Int Ed Engl* 48:344–347.
28. Baskin JM, et al. (2007) Copper-free click chemistry for dynamic in vivo imaging. *Proc Natl Acad Sci USA* 104:16793–16797.
29. Laughlin ST, Baskin JM, Amacher SL, Bertozzi CR (2008) In vivo imaging of membrane-associated glycans in developing zebrafish. *Science* 320:664–667.
30. Paige LA, Nadler MJ, Harrison ML, Cassady JM, Geahlen RL (1993) Reversible palmitoylation of the protein-tyrosine kinase p56lck. *J Biol Chem* 268:8669–8674.
31. Alland L, Peseckis SM, Atherton RE, Berthiaume L, Resh MD (1994) Dual myristylation and palmitylation of Src family member p59fyn affects subcellular localization. *J Biol Chem* 269:16701–16705.
32. Wolven A, Okamura H, Rosenblatt Y, Resh MD (1997) Palmitoylation of p59fyn is reversible and sufficient for plasma membrane association. *Mol Biol Cell* 8:1159–1173.
33. Bouvier M, et al. (1995) Dynamic palmitoylation of G-protein-coupled receptors in eukaryotic cells. *Methods Enzymol* 250:300–314.
34. Secrist JP, Burns LA, Karnitz L, Koretzky GA, Abraham RT (1993) Stimulatory effects of the protein tyrosine phosphatase inhibitor, pervanadate, on T-cell activation events. *J Biol Chem* 268:5886–5893.
35. Qanbar R, Bouvier M (2004) Determination of protein-bound palmitate turnover rates using a three-compartment model that formally incorporates [^{3}H]palmitate recycling. *Biochemistry* 43:12275–12288.
36. Zimmermann L, et al. (2010) Direct observation and quantitative analysis of Lck-exchange between plasma membrane and cytosol in living T cells. *J Biol Chem* 285: 6063–6070.
37. Kabouridis PS, Magee AI, Ley SC (1997) S-acylation of LCK protein tyrosine kinase is essential for its signalling function in T lymphocytes. *EMBO J* 16:4983–4998.
38. Zhang W, Trible RP, Samelson LE (1998) LAT palmitoylation: Its essential role in membrane microdomain targeting and tyrosine phosphorylation during T cell activation. *Immunity* 9:239–246.
39. Kosugi A, et al. (2001) A pivotal role of cysteine 3 of Lck tyrosine kinase for localization to glycolipid-enriched microdomains and T cell activation. *Immunol Lett* 76:133–138.
40. Hawash IY, et al. (2002) The oxygen-substituted palmitic acid analogue, 13-oxypalmitic acid, inhibits Lck localization to lipid rafts and T cell signaling. *Biochim Biophys Acta* 1589:140–150.
41. Li QJ, et al. (2004) CD4 enhances T cell sensitivity to antigen by coordinating Lck accumulation at the immunological synapse. *Nat Immunol* 5:791–799.
42. Duncan JA, Gilman AG (1998) A cytoplasmic acyl-protein thioesterase that removes palmitate from G protein alpha subunits and p21(RAS). *J Biol Chem* 273:15830–15837.
43. Duncan JA, Gilman AG (2002) Characterization of *Saccharomyces cerevisiae* acyl-protein thioesterase 1, the enzyme responsible for G protein alpha subunit deacylation in vivo. *J Biol Chem* 277:31740–31752.
44. Das AK, et al. (2000) Structural basis for the insensitivity of a serine enzyme (palmitoyl-protein thioesterase) to phenylmethylsulfonyl fluoride. *J Biol Chem* 275: 23847–23851.
45. Jennings BC, et al. (2009) 2-Bromopalmitate and 2-(2-hydroxy-5-nitro-benzylidene)-benzo[b]thiophen-3-one inhibit DHHC-mediated palmitoylation in vitro. *J Lipid Res* 50:233–242.
46. Resh MD (2006) Use of analogs and inhibitors to study the functional significance of protein palmitoylation. *Methods* 40:191–197.
47. Coleman RA, Rao P, Fogelsong RJ, Bardes ES (1992) 2-Bromopalmitoyl-CoA and 2-bromopalmitate: promiscuous inhibitors of membrane-bound enzymes. *Biochim Biophys Acta* 1125:203–209.
48. Beatty KE, et al. (2006) Fluorescence visualization of newly synthesized proteins in mammalian cells. *Angew Chem Int Ed Engl* 45:7364–7367.
49. Dieterich DC, Link AJ, Graumann J, Tirrell DA, Schuman EM (2006) Selective identification of newly synthesized proteins in mammalian cells using bioorthogonal noncanonical amino acid tagging (BONCAT). *Proc Natl Acad Sci USA* 103:9482–9487.
50. Baker TL, Zheng H, Walker J, Coloff JL, Buss JE (2003) Distinct rates of palmitate turnover on membrane-bound cellular and oncogenic H-ras. *J Biol Chem* 278: 19292–19300.